

一种改进型单光子雪崩二极管探测概率模型及验证

曹智祥, 曾美玲, 杨健, 金湘亮*

湖南师范大学物理与电子科学学院, 湖南 长沙 410081

摘要 基于半导体工艺器件仿真软件和 Matlab 编程, 对光子探测概率(PDP)进行了建模和实验表征。进一步考虑器件表面二氧化硅薄膜的光透射性, 可以准确预测单光子雪崩二极管(SPAD)的性能。将模拟结果与采用 $0.18 \mu\text{m}$ 标准双极-互补金属氧化物半导体-双重扩散金属氧化物半导体(BCD)工艺设计和加工的 SPAD 的结果进行比较。结果显示, PDP 的预测结果与实验结果之间具有良好的一致性, 平均误差为 1.72%。该模型可以减少商用器件仿真软件中存在的不收敛问题, 极大减少了开发 SPAD 器件新结构所需的时间和成本。

关键词 光电子学; 单光子雪崩二极管; 薄膜透射; 光子探测概率; Matlab 建模

中图分类号 O475 文献标志码 A

DOI: 10.3788/AOS222111

1 引言

可见光通信是利用荧光灯或者发光二极管等发出肉眼可见的明暗闪烁光信号来传输信息, 因此需要灵敏度高的接收器接收光信号。单光子探测器具有高灵敏度、高增益和大可见光宽谱段响应等优点, 在可见光通信领域有着极其重要的作用^[1-5]。因为双极-互补金属氧化物半导体-双重扩散金属氧化物半导体(BCD)工艺流程耗时且成本高昂, 所以单光子雪崩二极管(SPAD)性能预测对于制造前 SPAD 的优化设计至关重要。虽然商用半导体仿真软件通常可以模拟 SPAD 的电学特性, 如击穿电压、碰撞电离率、电场分布等, 但不能直接模拟 SPAD 的统计性能^[6-7]; 同时, 半导体仿真软件的内部运行机制不是公开的, 无法了解到详细的仿真过程, 而且在仿真过程中也容易发生不收敛现象。因此, 对 SPAD 性能参数的建模具有一定的现实意义。文献[8-11]提出了各种物理模型来计算基于一些物理机制的统计性能, 包括碰撞电离、载流子迁移率和载流子寿命等。事实上, 尽管有一些用于光子探测概率(PDP)计算的理论模型^[12-17], 但由于其物理过程复杂, 各种模型都存在较大的误差, 并在短波长范围内理论结果与实验结果不一致, 因此对 PDP 进行定量和可靠的预测一直是一项具有挑战性的工作。

本文提出并演示了一种 PDP 建模方法, 仅基于

BCD 制造参数来预测 SPAD 的 PDP。通过将商用半导体仿真软件获取的电场分布与依赖于位置的雪崩触发概率计算方法相结合, 考虑二氧化硅钝化层薄膜对入射光波长的影响, 模拟了与外加电压相关的 PDP。将预测结果与采用 $0.18 \mu\text{m}$ 标准 BCD 工艺设计和加工的 SPAD 的结果进行比较, 发现二者具有很好的一致性。该工作为设计和优化 BCD SPAD 的 PDP 提供了一种可行的方法, 对于提高器件的性能、减少器件开发时间和成本是至关重要的。

2 SPAD 器件结构与建模

2.1 器件结构

本文采用 P^+ /N 阵/深 N 阵的 SPAD 器件结构如图 1 所示, P^+ 和 N 阵交界处形成雪崩倍增区, 在 P^+ 区的上方引出阳极。在 N 阵两侧注入低浓度的 P 阵区作为器件的虚拟保护环, 虚拟保护环的引入主要用于防止边缘及表面过早击穿。在深 N 阵两侧的 N 阵上方注入高浓度的 N^+ 区并将其作为阴极引出, 以减小导通电阻。在 P 衬底两侧的 P 阵区上方注入高浓度 P^+ 区并将其作为衬底电极引出, 该 P^+ 区的作用与 N^+ 区相似。深 N 阵与 P 衬底形成一个反向 PN 结, 防止衬底产生的光生载流子扩散引起电荷串扰并影响器件的检测灵敏度^[18]。在盖革模式下, SPAD 在过大的偏置电压下工作, 其中 SPAD 的反向偏置电压大于击穿电压。光子

收稿日期: 2022-12-07; 修回日期: 2022-12-19; 录用日期: 2022-12-27; 网络首发日期: 2023-01-06

基金项目: 国家自然科学基金(62174052, 61827812)、湖湘高层次人才聚集工程(2019RS1037)、湖南省科技厅项目(2020GK2018)、湖南省研究生科研创新项目(QL20210131)

通信作者: *jinxl@hunnu.edu.cn

通过钝化层后被器件吸收,产生光生电子-空穴对。在中性区,电子和空穴通过扩散运动被耗尽区吸收,进而引发雪崩。在耗尽区,电子和空穴在高电场中以两个相反的方向加速,最终在耗尽区引发自持雪崩。在以下部分中,将对图1所示的SPAD器件的统计特性进行建模,并将模型计算结果与文献[19]中报道的测试数据进行比较。

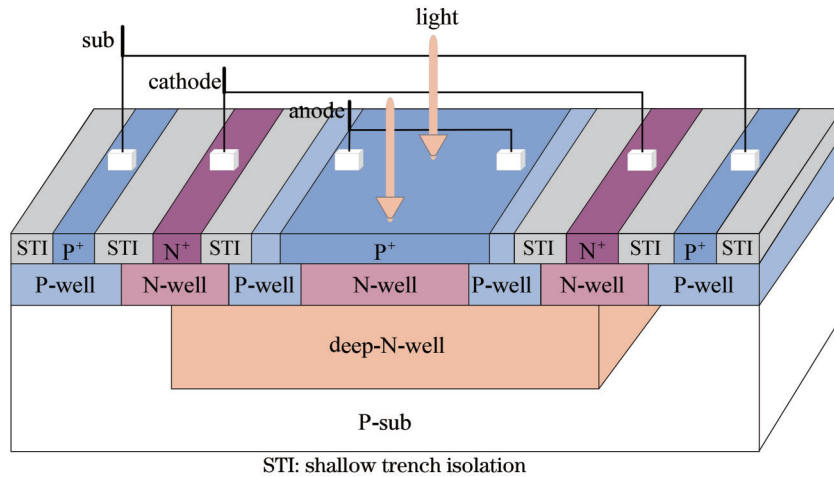


图1 P⁺/N阱/深N阱SPAD器件的三维结构示意图

Fig. 1 Schematic diagram of three-dimensional structure of P⁺/N well/deep N well SPAD device

2.2 PDP模型

PDP被定义为光子穿过硅表面二氧化硅层的光透射率和器件内部量子效率的乘积,器件内部量子效率是指光子被器件吸收并且产生雪崩触发的概率。P⁺/N阱/深N阱SPAD的内部量子效率分为三个部分,如图2所示。

在中性区(P)中,光子在SPAD顶部的P⁺层被吸收产生电子-空穴对,一些光生电子将扩散到耗尽区的上边界而没有被复合。这一过程发生的概率为

$$P_1 = \int_0^{w_1} f(x) g_1(x) dx, \quad (1)$$

式中: $g_1(x)$ 为光生电子到达耗尽区而没有发生复合的概率密度函数; w_1 为SPAD顶部到耗尽区上边界的深度; $f(x)$ 为光生载流子的概率密度函数,依赖于半导体中的光吸收系数 α ,可以表示为

$$f(x) = \alpha \exp(-\alpha x). \quad (2)$$

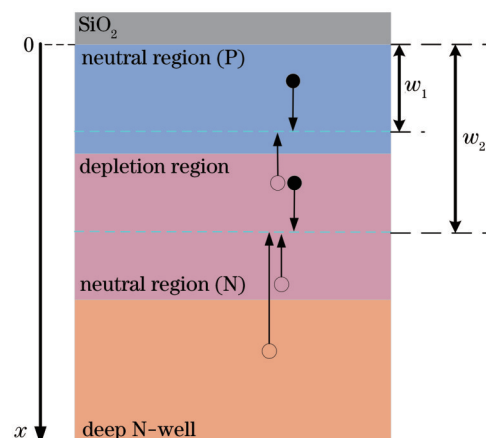


图2 光生电子-空穴对运动过程

Fig. 2 Movement process of photogenerated electron-hole pair

间接带隙半导体的吸收系数^[20]可以表示为

$$\alpha(\lambda, T) = \begin{cases} A \left[\frac{\left(\frac{hc}{\lambda} - E_g - E_p \right)^2}{\exp\left(\frac{E_p}{kT}\right) - 1} + \frac{\left(\frac{hc}{\lambda} - E_g - E_p \right)^2}{1 - \exp\left(\frac{E_p}{kT}\right)} \right], & hv \geqslant E_g + E_p \\ A \frac{\left(\frac{hc}{\lambda} - E_g - E_p \right)^2}{\exp\left(\frac{E_p}{kT}\right) - 1}, & E_g - E_p < hv < E_g + E_p \end{cases}, \quad (3)$$

式中: T 为热力学温度; v 为光子频率; λ 为入射光波长; h 为普朗克常量; c 为光速; k 为玻尔兹曼常数; E_g 为硅

材料的禁带宽度; E_p 为声子能量; A 为常数。光生电子到达耗尽区而没有发生复合的概率密度函数 $g_1(x)$ 为

$$g_1(x) = \exp[-(w_1 - x)/L_e], \quad (4)$$

式中: L_e 是电子扩散长度,可以表示为

$$L_e = \sqrt{D_n \tau_n}, \quad (5)$$

式中: D_n 是少子电子的扩散系数; τ_n 是少子电子的寿命。根据爱因斯坦关系式:

$$D_n = \frac{kT}{q} u_n, \quad (6)$$

式中: u_n 为少子电子迁移率; q 为单位电荷量。光生电子扩散到耗尽区并可能引发雪崩触发。因此,顶部P⁺层的内部量子效率 P_p 通过 P_1 和耗尽区边界 w_1 位置的电子雪崩触发概率 $P_e(w_1)$ 的乘积来计算:

$$P_p = P_1 P_e(w_1). \quad (7)$$

在耗尽区中,光生电子和空穴在耗尽区强电场的作用下以相反的方向漂移,并在运动极短的距离后引发雪崩触发,耗尽区的内部量子效率为

$$P_{dep} = \int_{w_1}^{w_2} f(x) P_{total}(x) dx, \quad (8)$$

$$P_{total}(x) = P_e(x) + P_h(x) - P_e(x) P_h(x), \quad (9)$$

式中: w_2 是器件顶部到高场区耗尽层底部的距离; $P_e(x)$ 和 $P_h(x)$ 分别是由位置 x 处的电子和空穴引发的雪崩触发概率; $P_{total}(x)$ 是 x 位置的电子或空穴引起雪崩触发的总概率。

在中性区(N)中,光生空穴可以在没有被复合的情况下到达耗尽区的底部并引发雪崩触发。该区域的

内部量子效率通过 P_2 和耗尽区边界 w_2 位置的电子雪崩触发概率 $P_h(w_2)$ 的乘积来计算,这一过程与中性区(P)的情况是极为类似的,为了方便起见,这里只给出最后的表达形式:

$$P_N = P_h(w_2) P_2 = P_h(w_2) \int_{w_2}^{\infty} f(x) \exp[-(x - w_2)/L_h] dx, \quad (10)$$

式中: P_N 为中性区(N)的内部量子效率; L_h 为空穴扩散长度。

需要指出的是,该积分区域不可能到 ∞ ,实际上是由空穴的扩散长度以及深N阱与P衬底形成的PN结深度所决定的。考虑上述三种情况及器件表面二氧化硅层透射系数 $T_r(\lambda)$,SPAD总的PDP(V_{PDP})为

$$V_{PDP} = T_r(\lambda) \cdot (P_p + P_{dep} + P_N). \quad (11)$$

2.3 模型实现

图3显示了PDP的实现步骤。首先将器件加工厂提供的掺杂浓度和设计的SPAD版图结构导入TCAD工具,重构二维器件模型。通过Sentaurus Sdevice自带的函数库,设置温度 T 、偏压 V_{bias} 、入射光波长 λ 等参数进行电学仿真,得到耗尽区电场强度 F 和耗尽区宽度 W 。然后将电场强度和耗尽区宽度导入Matlab软件构建的模型中,获取内部量子效率 Q_{in} 。利用粒子群优化算法获得二氧化硅薄膜钝化层透射光谱拟合参数 $T_r(\lambda)$,最后得到PDP。

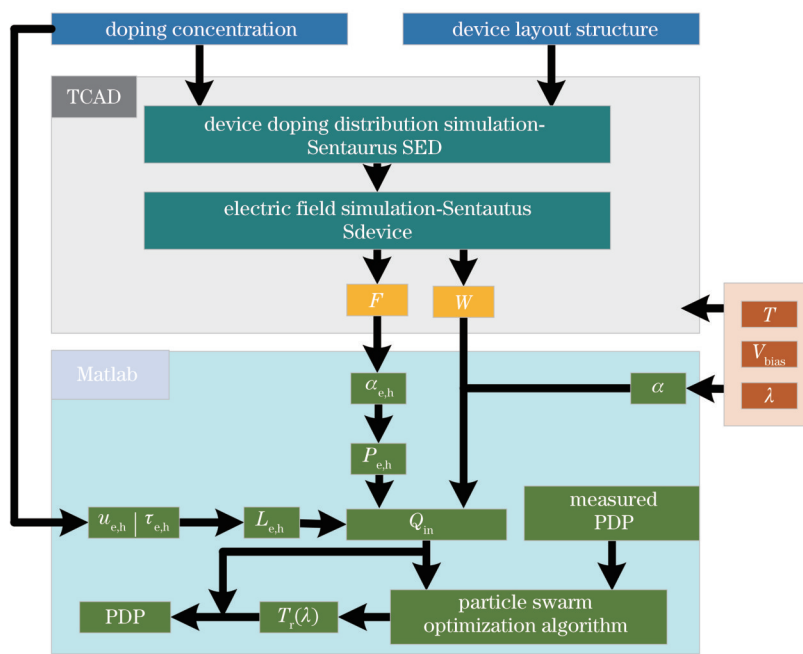


图3 PDP建模实现流程

Fig. 3 Realization process of PDP modeling

对于少数载流子迁移率($u_{e,h}$),采用Klaassen^[21]提出的多数载流子和少数载流子统一迁移率模型,该模型考虑了电荷载流子对杂质的屏蔽、电子和空穴散射、杂质的聚集以及载流子迁移率的温度依赖性,并给出

了相关解析函数。少数载流子寿命($\tau_{e,h}$)是对晶格缺陷的结构和密度以及杂质非常敏感的半导体参数之一,限制有效载流子寿命的两个主要因素是表面复合和俄歇过程,用掺杂浓度和温度依赖性建模^[22],该模型

引入载流子迁移率的温度依赖性,通过与实验数据比较拟合得到。电子和空穴的碰撞电离率有几种经验模型可用^[23-25]。在低电场下, van Overstraeten 和 de Man^[23]参数是最常用的,并与实验结果吻合良好。然而,本文所用器件在雪崩击穿时的电场峰值可以超过 5×10^5 V/cm,这超出了 van Overstraeten 和 de Man 表达式的有效范围上限。本文使用了 Okuto 和 Crowell^[25]经验表达式,该表达式体现温度依赖性,电场强度上限峰值达到 10×10^5 V/cm,而且与突变结二极管的实验结果非常一致。

半导体器件的制作一般会采用化学气相沉积法在器件表面沉积一层二氧化硅薄膜作为阻挡材料特定区域不被掺杂或离子注入,进而提高刻蚀反应的选择性。本文考虑二氧化硅钝化层薄膜对入射光波长的影响,对PDP的理论模型进行了改进。对理论模型与实验测试结果进行了比较,采用粒子群优化算法拟合出二氧化硅薄膜与波长相关的透射率,拟合的结果与二氧化硅薄膜测量的透射光谱^[26]具有一致性。拟合函数为

$$T(\lambda) = 1 - a_1 \exp\left[-\left(\frac{\lambda - b_1}{c_1}\right)^2\right] - a_2 \exp\left[-\left(\frac{\lambda - b_2}{c_2}\right)^2\right], \quad (12)$$

式中: $a_1 = 0.5165$; $a_2 = 0.8899$; $b_1 = 2.737 \times 10^{-7}$;

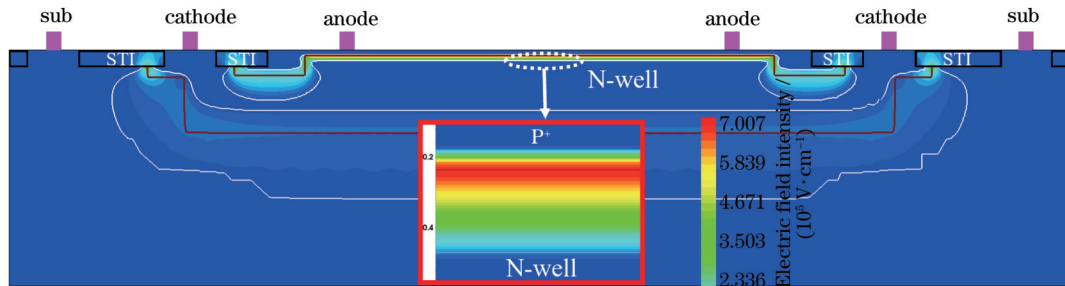


图4 P⁺/N阱/深N阱SPAD在1 V过偏压下的模拟二维电场分布

Fig. 4 Simulated 2D electric field distribution of P⁺/N-well/ deep N-well SPAD under 1 V overbias

图5显示了在1 V过偏压下的器件中心一维电场分布,横坐标表示器件表面到器件内部的深度,纵坐标表示电场强度。可以看到,电场分布符合突变结二极管加反向偏压的形式,电场强度在0.23 μm时达到峰值并向两边递减,在0.07 μm和0.52 μm时减小到 10^3 V/cm以下。图5中的插图表示商用器件仿真得到的器件电流-电压(I-V)特性,加在阴极的最终电压为12.7 V,这与1 V过偏压下的电场强度分布相对应。可以看出,器件在11.7 V左右发生了击穿现象,这与文献[19]的结果是一致的。

图6是分别在0.5、1.0、2.0、3.0 V过偏压下的电场分布,通过式(9)、(13)分别得到电子、空穴以及总的雪崩触发概率。随着过偏压的增加,耗尽区内部电场

$b_2 = 3.572 \times 10^{-7}$; $c_1 = 5.182 \times 10^{-8}$; $c_2 = 8.799 \times 10^{-8}$ 。

前文提到, P_e 和 P_h 分别为从耗尽区内触发电子和空穴雪崩的概率,是关于器件深度 x 的函数。令 α_e 和 α_h 分别表示电子和空穴的碰撞电离率,则电子和空穴的雪崩触发概率可以通过求解

$$\begin{cases} \frac{dP_e}{dx} = -(1 - P_e)\alpha_e(P_e + P_h - P_e P_h) \\ \frac{dP_h}{dx} = (1 - P_h)\alpha_h(P_e + P_h - P_e P_h) \end{cases} \quad (13)$$

得到,初始条件为 $P_e(w_2) = 0$, $P_h(w_1) = 0$ 。模型建立完成后,将模型仿真计算得到的PDP与实测结果进行比较,以验证模型的准确性。

3 仿真、测试结果分析

根据图1所示的P⁺/N阱/深N阱SPAD结构,首先使用Sentaurus SED基于标准0.18 μm BCD工艺进行了二维工艺模拟,通过工艺模拟获得SPAD器件结构。图4显示了在1 V过偏压(V_{ob})下SPAD的模拟二维电场分布。结果表明,具有强且均匀分布电场的雪崩倍增区(中间矩形框内深色区)位于P⁺/N阱结的中心区域。同时,雪崩倍增区域被明显较低的电场区域包围,这避免了PN结外围的过早击穿。为了与所报道的击穿电压^[19]相同,在进行工艺模拟时,略微调整了N阱的注入浓度。

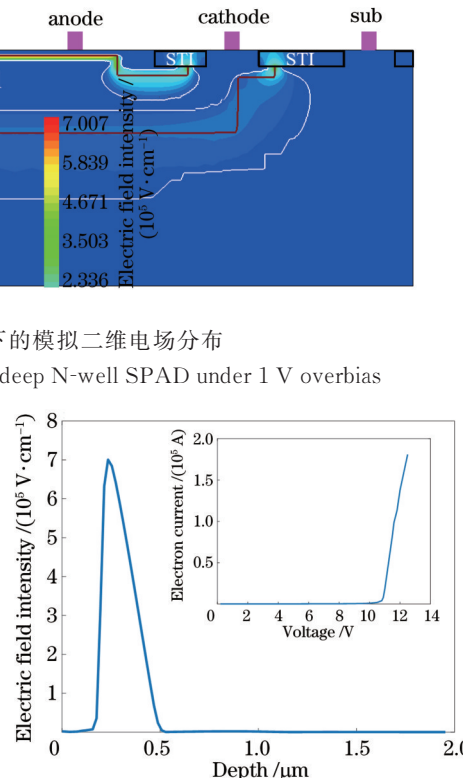


图5 1 V过偏压下通过Sentaurus Sdevice仿真获得的电场分布
Fig. 5 Electric field distribution obtained by Sentaurus Sdevice simulation under 1 V overbias

强度增强,导致电子、空穴的雪崩触发概率上升。雪崩触发概率是耗尽区内位置 x 的函数,其中图6(a)表示

电子的雪崩触发概率,图6(b)表示空穴的雪崩触发概率,图6(c)表示电子或空穴总的雪崩触发概率。

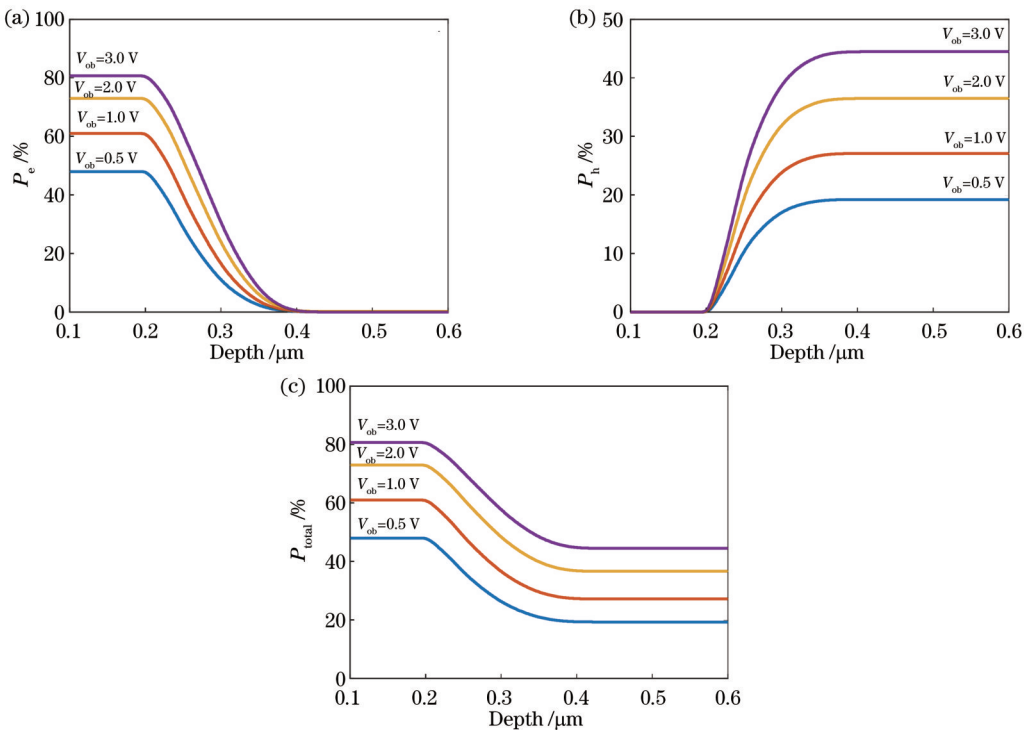


图6 耗尽区位置 x 处的电子和空穴雪崩触发概率。(a)电子雪崩触发概率;(b)空穴雪崩触发概率;(c)电子或空穴总的雪崩触发概率

Fig. 6 Avalanche triggering probabilities of electron and hole at depletion region location x . (a) Avalanche triggering probability of electron; (b) avalanche triggering probability of hole; (c) total avalanche triggering probability of electron or hole

图7显示了通过拟合得到的二氧化硅薄膜透射率随入射光波长的变化情况。透射率与入射光的波长、薄膜厚度以及二氧化硅纯度相关。从图7中可以看到,对于500 nm以下的短波长范围,二氧化硅薄膜透射率迅速下降,在300 nm波长几乎减小到0。这与实际情况是吻合的,因为入射光波长越短,入射光被一定厚度薄膜吸收的可能性越大。

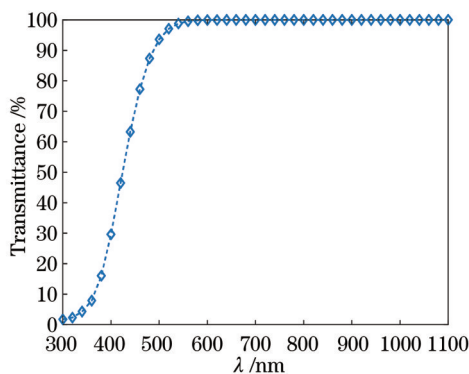


图7 二氧化硅薄膜的透射光谱

Fig. 7 Transmission spectrum of silica film

图8给出了在1 V过偏压下3个区域分别贡献的PDP仿真。其中,中性区(P)的贡献最大,其次是中性区(N),这种情况是合理的。中性区(P)贡献最大的原

因是其靠近硅表面,电子扩散长度一般在亚微米量级,几乎所有的光生电子都能够到达耗尽区上边界。而且,电子的雪崩触发概率比空穴的雪崩触发概率高。对于固定的入射光波长,入射光的吸收率随着入射深度的增大而降低。中性区(N)贡献较大是由深N阱大的宽度和空穴的几十微米扩散长度所决定的,这能够保证长波长产生的光生空穴更多地流入耗尽区下边界。

图9显示了在上述4种过偏压下总的PDP仿真结果。

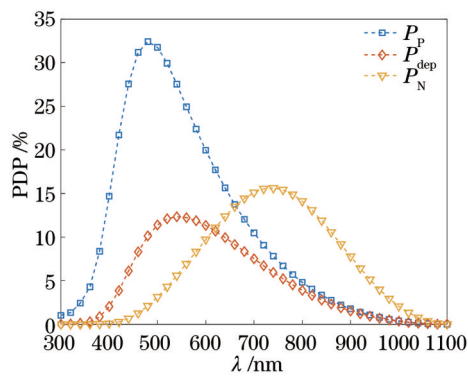


图8 中性区(P)、中性区(N)和耗尽区贡献的PDP

Fig. 8 PDP contributed by neutral region (P), neutral region (N), and depletion region

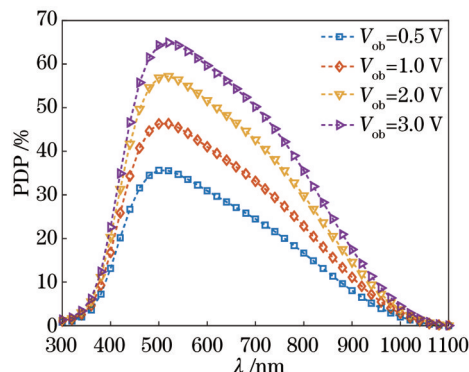


图9 PDP仿真结果

Fig. 9 Simulation results of PDP

图10为0.5 V过偏压下的PDP仿真与实测结果对比,可以看到,仿真模型模拟出的PDP与测试结果是基本吻合的。关于测试情况的描述,文献[19]已经给了清晰的描述,这里不再说明。平均误差定义为每个波长的绝对误差之和的平均值,则模型与实测的平均误差为1.72%,这种误差是由器件掺杂浓度随深度变化的不确定性以及电子、空穴扩散长度受缺陷影响的不确定性导致的。

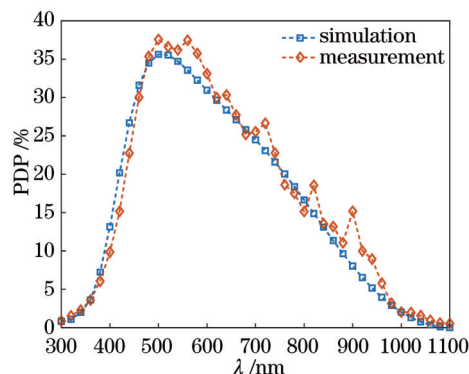


图10 0.5 V过偏压下的仿真与实测PDP

Fig. 10 Simulated and measured PDP under 0.5 V overbias

4 结 论

采用了Matlab建模方法来准确预测BCD SPAD的PDP,通过设计SPAD来验证模型预测结果。通过降低寄生电容、减少充电时间和避免过早的边缘击穿,实现了PDP测量。在没有衬底贡献的情况下,模拟0.5~3 V过偏压下的PDP,并且在0.5 V过偏压下比较了模型与实验测试结果,得到的平均误差只有1.72%。这种考虑二氧化硅钝化层薄膜透射光谱的PDP改进模型,为新型SPAD器件结构的开发提供了研究方向。

参 考 文 献

- [1] 万超,郝浩,赵清源,等.单光子探测在无线光通信收发技术中的应用[J].激光与光电子学进展,2022,59(5):0500001.
- [2] 尹涵,宋英雄,李迎春,等.基于MIMO模式分集相干接收的自由空间光通信大气湍流补偿技术研究[J].中国激光,2022,49(23):2306002.
- [3] Yin H, Song Y X, Li Y C, et al. Free-space optical communication atmospheric turbulence compensation based on multiple input multiple output mode diversity coherent reception [J]. Chinese Journal of Lasers, 2022, 49(23): 2306002.
- [4] 李琳,王超,郭家宁,等.基于删除Polar码的可调光可见光通信方案[J].光学学报,2022,42(16):1606007.
- [5] Li L, Wang C, Guo J N, et al. Dimmable visible light communication scheme based on punctured polar codes[J]. Acta Optica Sinica, 2022, 42(16): 1606007.
- [6] Mu Y, Wang C, Ren J W, et al. Evaluation and experimental comparisons of different photodetector receivers for visible light communication systems under typical scenarios[J]. Optical Engineering, 2021, 60(9): 096101.
- [7] Wen G H, Huang J, Zhang L, et al. A high-speed and high-sensitivity photon-counting communication system based on multichannel SPAD detection[J]. IEEE Photonics Journal, 2021, 13(2): 7900310.
- [8] Leitner T, Feiningstein A, Turchetta R, et al. Measurements and simulations of low dark count rate single photon avalanche diode device in a low voltage 180-nm CMOS image sensor technology[J]. IEEE Transactions on Electron Devices, 2013, 60(6): 1982-1988.
- [9] Bérubé B L, Rhéaume V P, Therrien A C, et al. Development of a single photon avalanche diode (SPAD) array in high voltage CMOS 0.8 μm dedicated to a 3D integrated circuit (3DIC)[C]// 2012 IEEE Nuclear Science Symposium and Medical Imaging Conference Record, October 27-November 3, 2012, Anaheim, CA, USA. New York: IEEE Press, 2012: 1835-1839.
- [10] Kindt W J, van Zeijl H W. Modelling and fabrication of Geiger mode avalanche photodiodes[J]. IEEE Transactions on Nuclear Science, 1998, 45(3): 715-719.
- [11] Kang Y, Lu H X, Lo Y H, et al. Dark count probability and quantum efficiency of avalanche photodiodes for single-photon detection[J]. Applied Physics Letters, 2003, 83(14): 2955-2957.
- [12] Mazzillo M, Piazza A, Condorelli G, et al. Quantum detection efficiency in Geiger mode avalanche photodiodes[J]. IEEE Transactions on Nuclear Science, 2008, 55(6): 3620-3625.
- [13] Chen C P, Tian M F, Jiang Z Y, et al. Improved two-dimensional responsivity physical model of a CMOS UV and blue-extended photodiode[J]. Journal of Semiconductors, 2014, 35(9): 094009.
- [14] Gulinatti A, Rech I, Fumagalli S, et al. Modeling photon detection efficiency and temporal response of single photon avalanche diodes[J]. Proceedings of SPIE, 2009, 7355: 73550X.
- [15] Pancheri L, Stoppa D, Dalla B G F. Characterization and modeling of breakdown probability in sub-micrometer CMOS SPADs[J]. IEEE Journal of Selected Topics in Quantum Electronics, 2014, 20(6): 328-335.
- [16] Hsieh C A, Tsai C M, Tsui B Y, et al. Photon-detection-probability simulation method for CMOS single-photon avalanche diodes[J]. Sensors, 2020, 20(2): 436.
- [17] 李丹妮,徐英添,徐莉,等. $In_{0.53}Ga_{0.47}As$ 光电探测器量子效率的理论仿真分析[J].光学学报,2015,35(12):1204002.
- [18] Li D N, Xu Y T, Xu L, et al. Theoretical simulation analysis the quantum efficiency of $In_{0.53}Ga_{0.47}As$ photodetectors[J]. Acta Optica Sinica, 2015, 35(12): 1204002.
- [19] Xu Y, Xiang P, Xie X P, et al. A new modeling and simulation method for important statistical performance prediction of single photon avalanche diode detectors[J]. Semiconductor Science and Technology, 2016, 31(6): 065024.

- [17] Moeini I, Ahmadpour M, Mosavi A, et al. Modeling the detection efficiency in photodetectors with temperature-dependent mobility and carrier lifetime[J]. *Superlattices and Microstructures*, 2018, 122: 557-562.
- [18] Wang Y, Jin X L, Cao S G, et al. Design and measurement of ring-gate single photon avalanche diode with low dark count rate [J]. *IEEE Photonics Journal*, 2020, 12(3): 1-11.
- [19] Zeng M L, Wang Y, Jin X L, et al. Design, fabrication, and verification of blue-extended single-photon avalanche diode with low dark count rate and high photon detection efficiency[J]. *Journal of Nanoelectronics and Optoelectronics*, 2021, 16(4): 546-551.
- [20] 刘恩科, 朱秉升, 罗晋生. 半导体物理学[M]. 7版. 北京: 电子工业出版社, 2008: 273-305.
Liu E K, Zhu B S, Luo J S. Semiconductor physics[M]. 7th ed. Beijing: Publishing House of Electronics Industry, 2008: 273-305.
- [21] Klaassen D B M. A unified mobility model for device simulation: I. Model equations and concentration dependence[J]. *Solid-State Electronics*, 1992, 35(7): 953-959.
- [22] Klaassen D B M. A unified mobility model for device simulation: II . Temperature dependence of carrier mobility and lifetime[J]. *Solid-State Electronics*, 1992, 35(7): 961-967.
- [23] van Overstraeten R, de Man H. Measurement of the ionization rates in diffused silicon p-n junctions[J]. *Solid-State Electronics*, 1970, 13(5): 583-608.
- [24] Grant W N. Electron and hole ionization rates in epitaxial silicon at high electric fields[J]. *Solid-State Electronics*, 1973, 16(10): 1189-1203.
- [25] Okuto Y, Crowell C R. Threshold energy effect on avalanche breakdown voltage in semiconductor junctions[J]. *Solid-State Electronics*, 1975, 18(2): 161-168.
- [26] 王铿, 贾宏志, 夏桂珍. 透射光谱法测试双面薄膜的光学参数[J]. 光谱学与光谱分析, 2008, 28(11): 2713-2716.
Wang K, Jia H Z, Xia G Z. Determination of optical parameters in thin films by transmittance spectra[J]. *Spectroscopy and Spectral Analysis*, 2008, 28(11): 2713-2716.

Detection Probability Model and Verification of an Improved Single-Photon Avalanche Diode

Cao Zhixiang, Zeng Meiling, Yang Jian, Jin Xiangliang*

School of Physics and Electronics, Hunan Normal University, Changsha 410081, Hunan, China

Abstract

Objective A method considering the light transmission of silicon dioxide film on the device surface can be proposed to address the large error between the existing photon detection probability (PDP) model and actual test results, which can accurately predict the detection probability of single-photon avalanche diodes (SPADs). Visible light communication requires a high-sensitivity receiver to receive optical signals, and single-photon detectors play an extremely important role in visible light communication because of their high sensitivity, high gain, and high visible light wide-spectrum response. Due to the time-consuming and cost-intensive bipolar-complementary metal oxide semiconductor-double diffusion metal oxide semiconductor (BCD) process workflow, prediction of SPAD performance is critical to optimize its design before fabrication. Although commercial semiconductor simulation software can usually simulate the electrical properties of SPADs, such as breakdown voltage, impact ionization rate, and electric field distribution, their statistical performance cannot be directly simulated. Additionally, since the internal operating mechanism of the semiconductor simulation software is not open, it is impossible to know the detailed simulation process, and it is also prone to non-convergence during the simulation. Therefore, it is of practical significance to model the performance parameters of SPADs. In fact, although there are some theoretical models for the calculation of PDP, due to the complex factors of its physical process, various models have large errors and are inconsistent with the experimental test trend in the short wavelength range. Thus, the photon-quantitative and reliable prediction of detection probability is challenging.

Methods The PDP is defined as the product of the light transmission of a photon passing through the silicon dioxide layer on the silicon surface and the internal quantum efficiency of the device. The internal quantum efficiency of the device is the probability triggered when a photon is absorbed by the device and results in an avalanche. The internal quantum efficiency of P^+ /N well/deep N well SPAD is divided into three parts. In the neutral region P, photons are absorbed in the P^+ layer on top of the SPAD to generate electron-hole pairs, and some photogenerated electrons will diffuse to the upper boundary of the depletion region, triggering an avalanche probability. In the depletion region, photogenerated electrons and holes drift in opposite directions under the action of a strong electric field in this region and trigger an avalanche after moving a very short distance. In the neutral region N, photogenerated holes can reach the bottom of the depletion region without being recombined, and initiate an avalanche trigger. In this study, the doping concentration provided by the device processing factory and the designed SPAD layout structure are imported into the TCAD tool to rebuild the two-dimensional device model. Through the function library that comes with Sentaurus Sdevice, parameters such as

temperature, bias voltage, and incident light wavelength are set for electrical simulation, and the electric field intensity and width of the depletion region are obtained. Then, the electric field strength and the width of the depletion region are imported into the model built by Matlab software to obtain the internal quantum efficiency. The particle swarm optimization algorithm is adopted to obtain the fitting parameters of the transmission spectrum in the passivation layer of the silicon dioxide film, and finally acquire the PDP.

Results and Discussions Firstly, two-dimensional process simulations are carried out through the Sentaurus SED based on the standard 0.18 μm BCD process and the SPAD device structure obtained from the process simulations. The simulated electric field distribution of the SPAD at an excess bias voltage of 1 V is simulated by Sentaurus Sdevice (Fig. 4) to extract the one-dimensional (1D) electric field distribution at the center of the device at an excess bias voltage of 1 V (Fig. 5). The electric field distributions at 0.5, 1.0, 2.0, and 3.0 V over-bias respectively are employed to calculate the avalanche trigger probability at each location in the depletion region (Fig. 6). The theoretical model of the PDP is improved by considering the effect of the silica passivation layer film on the incident light wavelength. The wavelength-dependent transmission of the silica film is fitted through a particle swarm optimization algorithm by comparing the theoretical model with experimental test results (Fig. 7). The PDPs contributed by each of the three components of the neutral P, depletion, and neutral N regions are calculated (Fig. 8), and the total PDP is the sum of the three components (Fig. 9). Finally, a PDP model with a low mean error is achieved (Fig. 10). The results show good agreement between the PDP predictions and experimental tests, with an average error of only 1.72%.

Conclusions We discuss the PDP for simulating typical over-bias voltages from 0.5 to 3 V without substrate contribution. The model and experimental test results are compared at the over-bias voltage of 0.5 V with an average error of only 1.72%. The average error is defined as the average of the sum of the absolute errors for each wavelength. The improved model for PDP considering the transmission spectrum of a thin film of silica passivation layer provides a research direction for the development of new SPAD device structures. Results show that the model can reduce the non-convergence problems in commercial device simulation software, and greatly reduce the time and cost required to develop new structures for SPAD devices. Additionally, the building of models for electric field strength, avalanche trigger probability, and carrier lifetime can help dark counting analysis, thus enlightening related researchers.

Key words optoelectronics; single-photon avalanche diode; film transmission; photon detection probability; Matlab modeling